IEEE Access
Multidisciplinary ⋮ Rapid Review ⋮ Open Access Journal

Received 14 December 2022, accepted 8 February 2023, date of publication 22 February 2023, date of current version 27 April 2023.

Digital Object Identifier 10.1109/ACCESS.2023.3246731

RESEARCH ARTICLE

Development and Analysis of a Multimaterial FDM 3D Printed Capacitive Accelerometer

GIANLUCA BARILE, PAOLO ESPOSITO, VINCENZO STORNELLI, (Senior Member, IEEE), AND GIUSEPPE FERRI, (Senior Member, IEEE)

Dipartimento di Ingegneria Industriale e dell'Informazione, University of L'Aquila, 67100 L'Aquila, Italy

Corresponding author: Vincenzo Stornelli (vincenzo.stornelli@univaq.it)

This work was supported by the Società Italiana di Elettronica (SIE).

ABSTRACT Nowadays quick fabrication of mechanical spare and replacement has become more and more necessary. This is the main reason why rapid prototyping and additive manufacturing has spread in several fields, including sensor manufacturing. In this work, we propose a Fused-Deposition-Fabricated Electro-Mechanical System (FDFEMS) accelerometer sensor. As the name suggests, it was implemented with Fused Deposition Modelling (FDM) additive manufacturing and material switching capabilities of the E3D ToolChanger motion platform. Fabrication process is based on insulating plastic to implement the mechanical structure of the device, conducting plastic to manufacture the actual differential capacitance sensing element and soluble material for sacrificial scaffolding. Together with the accelerometer, we also propose a novel fully differential interface circuit for differential capacitive sensors, based on the autobalanced bridge theory where capacitive sensor variations are balanced through voltage-controlled impedances placed in the bridge branches. Measurements from the sensor system were compared to theoretical values, showing good agreement. Furthermore, these measurements were repeated with different sensors and different test masses, to determine variations of the parameters evaluated. Specifically, measured sensitivity, damping factor and quality factor, with a fill factor of 100%, have resulted equal to 0.201 V/g, 0.055, and 9.042, respectively. It was then observed that the decrease of the proof mass fill factor led to a higher sensor resonant frequency, hence a wider flat band region in the frequency response, with decreased sensitivity and resolution. Mainly, this paper aims to evaluate and discuss the feasibility of the 3D printing Fused Deposition Modelling technique for manufacturing accelerometer sensors and classify sensor parameters as a function of its internal density, that is an easily selectable parameter for this kind of modelling.

INDEX TERMS 3D print, sensor interfaces, 3D printed electronic, 3D printed sensor, multi-material 3D print.

I. INTRODUCTION

Accelerometers are transducers that return the acceleration value of an object in static conditions, e.g. remaining stationary on a surface, or in dynamic conditions, e.g. when undergoing shock and stress at a certain frequency.

These devices are very useful as they allow to extract, from the measured acceleration, important data like the orientation of the object in the space (in static conditions) and the magnitude of the stress (dynamic) suitable for a further analysis.

The associate editor coordinating the review of this manuscript and approving it for publication was Michail Kiziroglou.

Nowadays, accelerometer systems are used in a wide range of applications, as in the field of Structural Health Monitoring (SHM), a discipline that studies the observation and analysis of heavy architectural structures, like buildings or bridges, with the aim of preserving their structural integrity: accelerometers define very important parameters like the building response in case of earthquakes, considered as dynamic input waves. In this regard, the literature available is wide, spacing from applications that involve wireless sensors to applications where accelerometer systems are combined with other important elements, like GPS or cameras (with post-processing techniques) [1], [2], [3], [4].

Another application field for accelerometer sensors is biology, in particular the study of livestock diseases: in this case, accelerometers are used to monitor large movements when suffering from a particular disease or condition (e.g. mold contaminated feed, ephemeral fever) [5], [6].

Other interesting applications which involve accelerometer sensors concern: monitoring application in industrial field (tool condition monitoring) [7], fault detection procedures for electric motors [8], pattern recognition through smartphone integrated accelerometers [9], their usage on wearable devices for fitness-tracking applications [10].

Concerning the main fabrication techniques, as reported in [11], production processes that are still the most widespread today for construction of standard accelerometer devices are surface and bulk micromachining. They are processes where microstructures, like mass-spring systems (internal characteristic structure of an accelerometer), are built through etching over or inside a substrate respectively. Nevertheless, nowadays alternative methods for the construction of new accelerometer systems are being developed, based on wet anisotropic etching with KOH [12], BiCMOS-adapted surface micromachining [13], [14], [15] and production methods which ease the integration with CMOS technology [16], in parallel with brand new processes for the development of internal springs, made with specific polymer material [17], or with specific spring structures [18].

However, as far as the listed above techniques allow to obtain accelerometers with a high precision and a minimized area, unfortunately they are time-consuming: another trend linked to today-sensor devices, which is increasing more and more, is the rapid prototyping, that is a set of techniques (like 3D printing) for manufacturing components or entire systems designed through Computer Aided Design (CAD). The main advantage of these methods is the easiness of substituting faulty mechanical or electrical pieces, speeding up the troubleshooting in a remarkable way.

This trend can be seen also in the electronics environment. Indeed, as reported in [19], several 3D printed sensors have been manufactured in a wide range of fields, even though with some concerns on printing materials (both for performance and environmental sustainability), life cycle, nanoparticles usage.

Nevertheless, several 3D printed accelerometers have been already introduced in the literature [19], [20], [21], [22]. In particular, in [21] Arh et al. have fabricated an uniaxial piezoresistive accelerometer based on the analytical beam theory using fused-deposition modelling as manufacturing process, obtaining a sensitivity up to 15 μV s^2/m, with a maximum solicitation frequency of 525 Hz, solution that was further developed by the same authors in [22], where a triaxial piezoresistive accelerometer sensor manufactured with E3D ToolChanger 3D printer reached a sensitivity up to 15 mΩm/s^2 with solicitation frequency between 20 and 150 Hz. Although these results were very good for a Fused Deposition Modelled (FDM) printed accelerometer, demonstrating that FDM is a good alternative for piezoresistive accelerometers manufacturing, piezoresistive accelerometers are highly temperature sensitive, which is a peculiarity that limits the environmental spectrum where these sensors can be used.

Further interesting work is performed by Zega et al. [20], where a triaxial accelerometer based on differential capacitance sensing is firstly printed through stereolitography, to be then entirely wet metalized with copper, in order to become totally conductive, through two different processes which differ in copper thickness and electrolytic percentage. This implementation ensures a major step forward in sensor manufacturing, as the proposed sensor form can implement differential capacitance based accelerometers, however it leverages stereolithography as a 3D printing method, which is still a good point for high resolutions, but it requires a cumbersome post processing of the 3D printed structure.

Considering the novel implementation by Zega et al. and previous 3D printed sensor implementations [23], in this work we propose a differential capacitance-based accelerometer sensor printed with the FDM technique. This work is a consistent upgrade from a previous study [24], which involves the usage of a multi-tool multi-material 3D printing technique and the development of a fully differential electronic interface to increase capacitance to voltage conversion performances.

The aim of this paper is to characterize the proposed sensor structure at different fabrication fill-factors. This activity is necessary to verify the conformity of a FDM 3D printed sensor behavior at different fabrication conditions if compared to the traditional MEMS accelerometers so to replace, in the future, general purpose devices with application-tailored counterparts. The proposed 3D printed sensor is then integrated with a novel fully differential electronic interface that represents an evolution of those proposed from Depari et al. [25].

This work is divided as follows. Section II introduces the operating principle of the sensor, deepening its mechanic structure, materials, and acceleration measurement. Sensor front-end circuitry design, development and measurements are discussed in section III, while printed sensor results are reported in section IV. Finally, conclusions and possible further works are listed in Section V.

II. MATERIALS AND METHODS

In this section, the design and fabrication of the proposed sensor, as well as its electronic interface are discussed, to introduce their working principle and explain how the measurements were performed.

A. ELECTRONIC INTERFACE

The proposed readout circuit is based on a modified De Sauty auto-balanced bridge (see Fig. 1). The feedback loop is performed via the synchronous demodulation technique. The sensor capacitors are arranged on the two upper sides of the bridge, while voltage Controlled Capacitors (VCCs) are used to complete its lower sides.

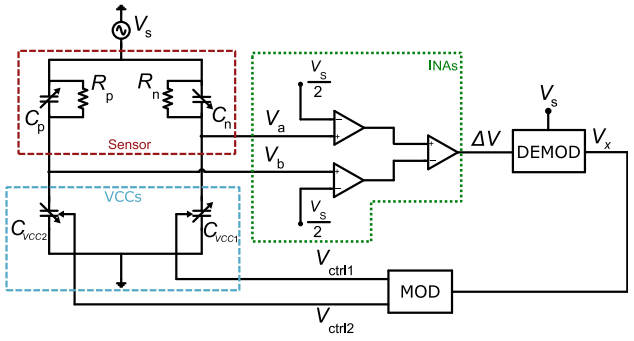

FIGURE 1. Proposed sensor interface: the autobalanced bridge is made of the sensor (upper side, highlighted in red) and two VCCs (lower side). Three INAs (highlighted in green) extract the error signal that is then processed by the DEMOD/MOD feedback path.

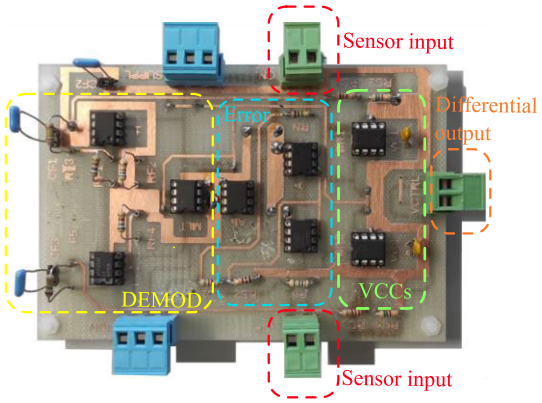

FIGURE 2. Fabricated electronic interface board, where the different processing sections are highlighted.

Differently form previous works [25], [26], [27], [28], this arrangement makes it possible to maintain a fixed common-mode voltage on both branches of the bridge, thus increasing the linearity of the feedback circuitry. In addition to this, the positioning of the sensor allows for a true fully differential output.

Considering the circuit shown in Fig.1, it is possible to divide it in three different parts: the first includes the bridge and three instrumentation amplifiers (INAs), the second is composed by a demodulator and the third consists of a modulator.

The bridge is excited by a sinusoidal voltage $v_s(t)$. The first couple of INAs compares the output of the bridge to a reference signal so to ensure that the feedback circuitry balances the bridge at the correct common mode value. On the other hand, the third INA calculates the feedback error voltage $\Delta v(t)$ between the two bridge outputs. This error is equal to zero at the steady state.

The demodulator is used to produce a baseband signal component linked to the pass-band sinusoidal error voltage $\Delta v(t)$, whose frequency and phase are the same as the excitation voltage $v_s(t)$. This function is obtained using an analog multiplier whose inputs are $\Delta v(t)$ and $v_s(t)$ so that at the output of the multiplier we have:

$$v_x(t) = \frac{\Delta V \cdot V_s}{2} \cdot [1 - \cos(\omega t)] \tag{1}$$

Lastly, the modulator has the double function to control the feedback loop, therefore compensating the error voltage, and to filter the previously introduced baseband component resulted from the demodulation. From a circuit point of view, it is possible to use a simple voltage integrator can be used implementing a purely integral compensation. The output values of the interface can be evaluated as:

$$V_{ctrl1} = -10 \cdot x \tag{2}$$

$$V_{ctrl2} = 10 \cdot x \tag{3}$$

The aforementioned circuit was fabricated via discrete components and is shown in Fig. 2. Specifically, AD633s were used to implement the variable capacitors (Zhong configuration [29]), an AD633 was also used as analog multiplier in the demodulator circuit, an INA128 was used as instrumentational amplifier, and LF411 circuits as operational amplifier.

B. SENSOR FABRICATION

The main principle behind the choice of the sensor shape is to maintain a high symmetry among the three axes in order to achieve an equal response in every solicitation direction.

Considering this requirement, sensor shape reproduces that one proposed by Zega et al. in [20], where a cubic structure hosts a six-faced proof mass free to move in all the directions and connected to the chassis through springs. Although the FDM technology presents a reduced fabrication accuracy as compared to other additive processes such as stereolithography, it has many advantages, namely the possibility of choosing the most suitable materials according to the application, and the feasibility of combining multiple materials during the same manufacturing phase. An advantage of manufacturing the shape via a multi-tool, multi-material process is twofold, on the one hand it is possible to accurately assign conductive/insulating properties to each face, opposed to the metallization process that involves each surface regardless, on the other hand it is possible to achieve a true hyperbolic differential capacitor for each of the three axes, further reducing their insulation.

In Fig. 3, the working principle of the differential capacitances is represented: the discussed sensor hosts an hyperbolic differential capacitive structure for each axis; this means that differential capacitances Cp, Cn, which have complementary values, change their capacitance in function of the plates distance, which in turn varies due to the movements of the mobile intermediate plate towards one of the boundary plates. The behavior of the sensor can be described as a function of an dimensionless parameter called $x = (C_p - C_n)/(C_p + C_n)$ [25]:

$$Cp, n = \frac{Cbl}{(1 \mp x)} \tag{4}$$

Cbl is the baseline capacitance value, that is the value of Cp,n when no solicitation is applied to the sensor. As previously

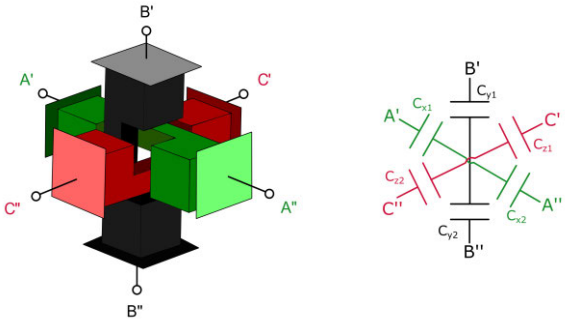

FIGURE 3. Fabricated electronic interface board.

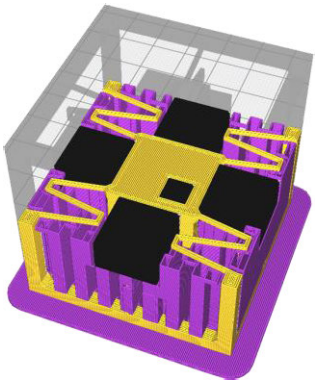

FIGURE 4. Materials distribution for each sensor surface: in yellow insulating structures and springs, in black conductive sensor surfaces and in purple, soluble sacrificial supporting structures.

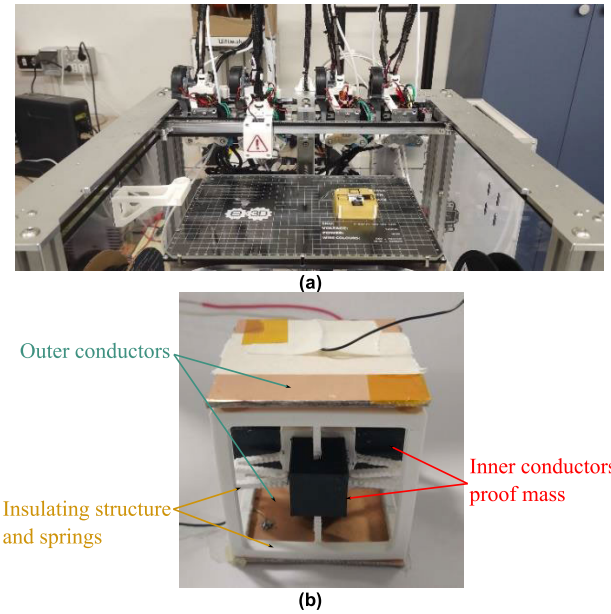

FIGURE 5. Proposed sensor: (a) highlight on the ToolChanger fabrication process, (b) complete device, with external electrodes covering a single axis.

reported, each of the six faces of the proof-mass form the differential capacitor mobile plate, while external plates are realized through the application of electrodes on each face of the cubic frame, obtaining a baseline capacitance of about 9 pF, from a distance between mass and electrode that reaches 0.2 mm. The proof mass is made of a conductive core, implemented via Protopasta Conductive filament, a blend of Polylactic Acid (PLA) and carbon black, and simple PLA for the insulating structure that holds the conductors and electrically separates them. Springs and chassis are also implemented via simple insulating PLA. As a proof of concept, with no specific applications, these materials were chosen so to be compatible one each other (i.e. they adhere one each other), however, it is remarkable that material choice can be adequately studied according to each specific use-case. Support structures were printed in Polyvinyl Alcohol (PVA), that is a water-soluble material and allows to easily remove them after the print by simply dipping the sensor in tap water. This is a great advantage since makes the sensor readily available after the printing process and minimizes the needed post processing. In Fig. 4 the introduced materials distribution within the sensor is represented: Protopasta Conductive filament is pictured as the black section, while yellow section represents PLA manufactured parts, and finally PVA is described by the purple section.

Sensors were printed with the E3D Tool Changer platform. Since it is a multi-tool platform, it is possible to use different tools for each material, therefore minimizing oozing and mixing of the different materials. A picture of the fabrication process is reported in Fig. 5a, while a detail on the final sensor is shown in Fig 5b.

C. MEASUREMENT SETUP

Measurement setup is intended both for the electronic interface measurements and sensor characterization

In the first case, a Keysight 33600A waveform generator, a Keysight MSOX3054T oscilloscope, and a Keysight E36313A continuous voltage source are used: measurements on the interface were performed considering known values of parameter x, hence known values of Cp and Cn equivalent capacitances, which vary from −0.9 to 0.9 with a 0.1 increment. Results from these measurements are the (Vctrl1,Vctrl2) versus x characteristics so that it could be compared to a mathematical calculated model. In the second case, a more complex setup is arranged, containing the same measurement instruments listed above but with the additional sensor, equipped with its six electrodes, that act as the six external differential capacitors contacts, which is placed above a speaker (with suitable stimulus mechanical transmission system) connected to the waveform generator to vary waveform, amplitude and frequency. An ADXL355 MEMS accelerometer was used as a reference in order to accurately measure accelerations and frequencies.

In the sensor characterization, the following experiments were performed:

1. pulse response, where sensor is solicited with a 1g pulse stimulus, calculating sensor resonance frequency, damping factor and Q factor;

2. frequency response, where sensor is solicited with a variable frequency sinusoidal wave, in the small-signal domain

TABLE 1. Main parameters versus fill factor.

Parameter	10% infill	50% infill	100% infill
Sensitivity	0.005 V/g	0.045 V/g	0.2009 V/g
Resolution	100 mg	80 mg	20 mg
f_n	20.086 Hz	20.03 Hz	17.761 Hz
BW	16 Hz	15 Hz	10 Hz
Q	5.3975	9.0423	8.6278
Maximum linearity error	26.6 %	19.4 %	4.8 %

(0.1g), validating resonant frequency and observing the flat-band part of its response;

3. input-output (I/O) characteristic, where sensor input is a in-band fixed frequency sinusoid, with variable amplitude (reported in g) in order to obtain the sensor linearity and sensitivity.

These tests were performed for each manufactured sensor, whose difference is the fabrication fill factor, hence internal mass density, equal to 100%, 50% and 10% (percentage between material and air), extracting the aforementioned values from the reading of $Vout = Vctrl1 - Vctrl2$.

III. RESULTS

In this section, we report results related to interface with respect to fixed measurand values and sensor characterization.

A. INTERFACE MEASUREMENTS

To confirm measured values and compare them with a suitable characteristic, we used as reference eq.(2) and eq.(3), where a theoretically linear relationship between control voltages and x parameter is shown. Interface measurements were then performed considering the setup above defined, and obtaining the result represented in Fig. 6. From Fig. 6 we notice a good agreement between theoretical and measured values, in particular a saturation of the two voltage is noticed when they reach ± 9.6 V, for $x < -0.9$ and $x > 0.8$.

This is mainly due to the non-ideal behavior of the Zhong VCC that is not able to reach very small capacitance values that are reached at the boundaries of the x values.

Another non ideal behavior of the measured I/O characteristic is its gain error. This is caused by the effects of parasitic capacitances placed between the outputs of the bridge and ground.

The full-scale error between measured values and theoretical behavior remains below 5% full-scale.

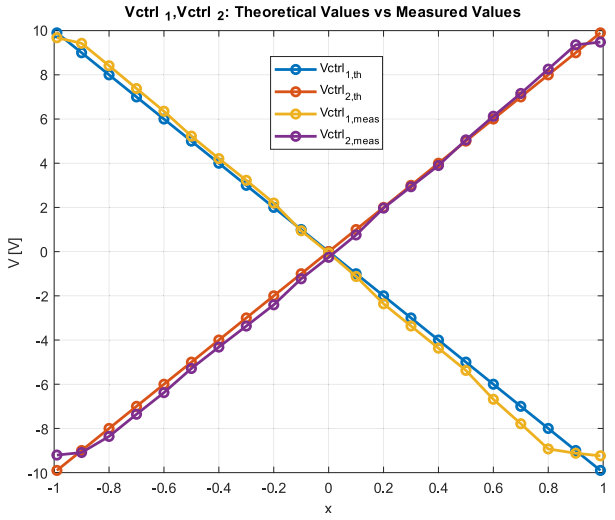

FIGURE 6. Fabricated electronic interface board.

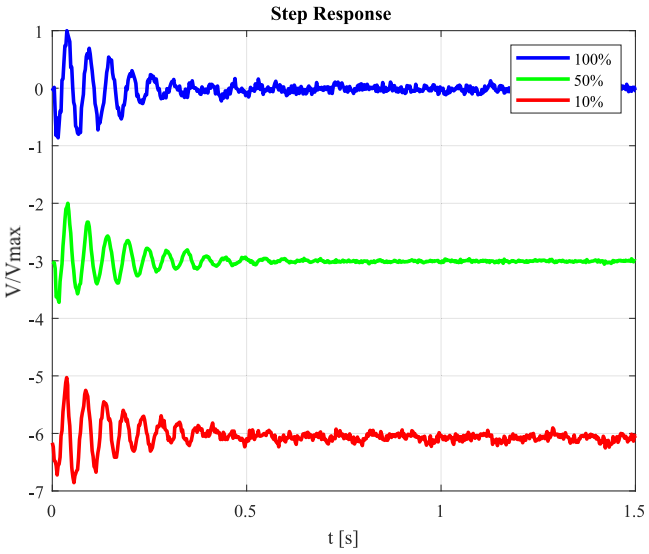

FIGURE 7. Normalized step response at three different fill factors.

Both of the non idealities can be neglected easily compensated when using the interface in conjunction with the proposed sensor.

B. SENSOR CHARACTERIZATION

From the sensors normalized step response, reported in Fig. 7, we see that, as expected, the lowering of mass density leads to a higher resonant frequency, as its mass decreases.

Sensor frequency response is shown (Fig. 8). In these responses, as expected, there is a clearer view of the previously extracted natural frequency variation, exactly as the flat band region, whose width is enlarged as the masses density decreasing. We remark that frequency response increment slows down as the mass density decreases.

Final measurements regard the I/O characterization of manufactured sensors: linearity, sensitivity and resolution are shown in Fig. 9.

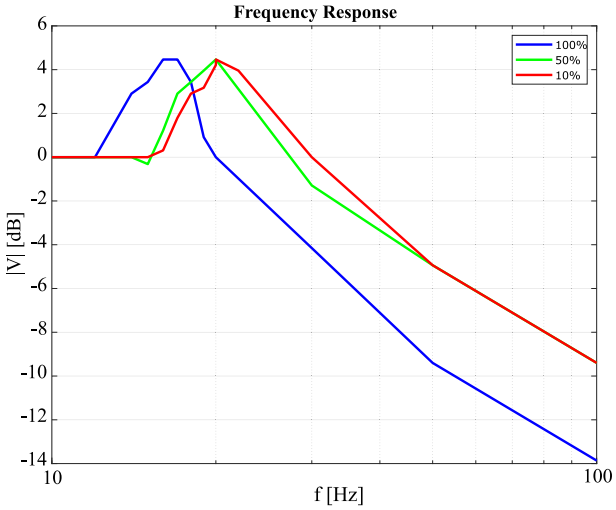

FIGURE 8. Sensor frequency response.

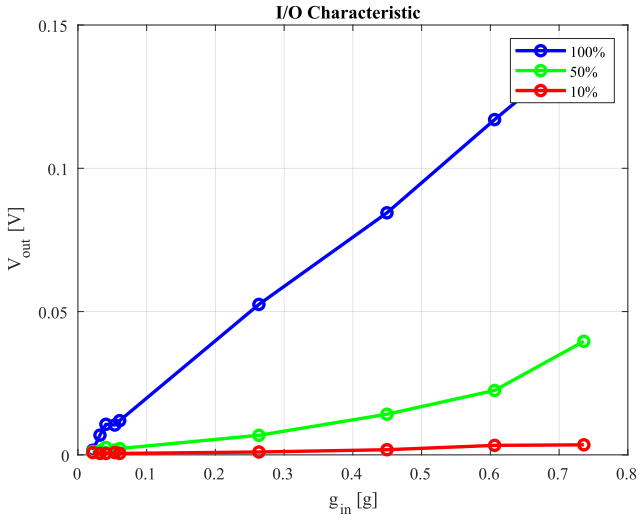

FIGURE 9. Sensors I/O characteristics.

As reported in Fig. 9, where the gravitational acceleration was neglected, the I/O characteristic slope increases as the proof mass percentage increases, resulting in a higher sensitivity. Sensor linearity, calculated by performing a linear regression of output values and comparing this ideal characteristic to the real one, shows that, according to the previous quantities, linearity falls as we decrease sensor mass. Dynamic range of the sensor was not evaluated due to the impossibility of producing a large enough acceleration. Table 1 summarizes the achieved results.

IV. CONCLUSION

In this work we have shown the process of developing, characterization and comparison of a 3D printed accelerometer paired with a custom fully differential electronic interface. We believe that results coming from this work prove the feasibility of directly manufacturing a capacitive accelerometer by using the FDM multi material technique. This is relevant because it gives the remarkable flexibility to tailor the sensor shape, performances, and materials specifically for a given application. We believe that, in the future, direct sensor will allow the sensing element to be incorporated directly into mechanical systems allowing quantities to be measured that would otherwise be impossible to directly evaluate. Moreover, it will be interesting to investigate the possibility of a monolithic 3D printed sensor and interface, combining both sensor and electronic interface directly onto the same 3D printed substrate.

REFERENCES

[1] P. Ragam and N. D. Sahebraoji, "Application of MEMS-based accelerometer wireless sensor systems for monitoring of blast-induced ground vibration and structural health: A review," *IET Wireless Sensor Syst.*, vol. 9, no. 3, pp. 103–109, Jun. 2019.

[2] Y. Xu, J. M. W. Brownjohn, and F. Huseynov, "Accurate deformation monitoring on bridge structures using a cost-effective sensing system combined with a camera and accelerometers: Case study," *J. Bridge Eng.*, vol. 24, no. 1, Jan. 2019, Art. no. 05018014.

[3] C. Bedon, E. Bergamo, M. Izzi, and S. Noè, "Prototyping and validation of MEMS accelerometers for structural health monitoring—The case study of the Pietratagliata cable-stayed bridge," *J. Sensor Actuator Netw.*, vol. 7, no. 3, p. 30, Jul. 2018.

[4] M. R. Kaloop and H. Li, "Tower bridge movement analysis with GPS and accelerometer techniques: Case study Yonghe tower bridge," *Inf. Technol. J.*, vol. 8, no. 8, pp. 1213–1220, Nov. 2009.

[5] S. C. Gurule, V. V. Flores, K. K. Forrest, C. A. Gifford, J. C. Wenzel, C. T. Tobin, D. W. Bailey, and J. A. H. Gifford, "A case study using accelerometers to identify illness in ewes following unintentional exposure to mold-contaminated feed," *Animals*, vol. 12, no. 3, p. 266, Jan. 2022.

[6] C. Tobin, D. W. Bailey, M. G. Trotter, and L. O'Connor, "Sensor based disease detection: A case study using accelerometers to recognize symptoms of bovine ephemeral fever," *Comput. Electron. Agricult.*, vol. 175, Aug. 2020, Art. no. 105605.

[7] G. Serin, B. Sener, A. M. Ozbayoglu, and H. O. Unver, "Review of tool condition monitoring in machining and opportunities for deep learning," *Int. J. Adv. Manuf. Technol.*, vol. 109, nos. 3–4, pp. 953–974, Jul. 2020.

[8] C. Cristalli, N. Paone, and R. M. Rodríguez, "Mechanical fault detection of electric motors by laser vibrometer and accelerometer measurements," *Mech. Syst. Signal Process.*, vol. 20, no. 6, pp. 1350–1361, Aug. 2006.

[9] A. Bujari, B. Licar, and C. E. Palazzi, "Movement pattern recognition through smartphone's accelerometer," in *Proc. IEEE Consum. Commun. Netw. Conf. (CCNC)*, Jan. 2012, pp. 502–506.

[10] A. Jalal, M. A. K. Quaid, S. B. U. D. Tahir, and K. Kim, "A study of accelerometer and gyroscope measurements in physical life-log activities detection systems," *Sensors*, vol. 20, no. 22, p. 6670, Nov. 2020.

[11] M. Kraft, "Micromachined inertial sensors: The state-of-the-art and a look into the future," *Meas. Control*, vol. 33, no. 6, pp. 164–168, Jul. 2000.

[12] S. Butefisch, A. Schoft, and S. Buttgenbach, "Three-axes monolithic silicon low-g accelerometer," *J. Microelectromech. Syst.*, vol. 9, no. 4, pp. 551–556, Dec. 2000.

[13] W. Kuehnel and S. Sherman, "A surface micromachined silicon accelerometer with on-chip detection circuitry," *Sens. Actuators A, Phys.*, vol. 45, pp. 7–16, Oct. 1994.

[14] M. Offenberg, F. Larmer, B. Elsner, H. Munzel, and W. Riethmuller, "Novel process for a monolithic integrated accelerometer," in *Proc. Int. Solid-State Sens. Actuators Conf. TRANSDUCERS*, vol. 95, vol. 1, 1995, pp. 589–592.

[15] T. Konishi, D. Yamane, T. Matsushima, G. Motohashi, K. Kagaya, H. Ito, N. Ishihara, H. Toshiyoshi, K. Machida, and K. Masu, "Novel sensor structure and its evaluation for integrated complementary metal oxide semiconductor microelectromechanical systems accelerometer," *Jpn. J. Appl. Phys.*, vol. 52, no. 6S, Jun. 2013, Art. no. 06GL04.

[16] K. H.-L. Chau, S. R. Lewis, Y. Zhao, R. T. Howe, S. F. Bart, and R. G. Marcheselli, "An integrated force-balanced capacitive accelerometer for low-g applications," *Sens. Actuators A, Phys.*, vol. 54, nos. 1–3, pp. 472–476, Jun. 1996.

[17] J. C. Lötters, W. Olthuis, P. H. Veltink, and P. Bergveld, "Polydimethylsiloxane as an elastic material applied in a capacitive accelerometer," *J. Micromech. Microeng.*, vol. 6, no. 1, pp. 52–54, Mar. 1996.

[18] H. Zhang, X. Wei, Y. Ding, Z. Jiang, and J. Ren, "A low noise capacitive MEMS accelerometer with anti-spring structure," *Sens. Actuators A, Phys.*, vol. 296, pp. 79–86, Sep. 2019.
[19] M. R. Khosravani and T. Reinicke, "3D-printed sensors: Current progress and future challenges," *Sens. Actuators A, Phys.*, vol. 305, Apr. 2020, Art. no. 111916.
[20] V. Zega, M. Invernizzi, R. Bernasconi, F. Cuneo, G. Langfelder, L. Magagnin, M. Levi, and A. Corigliano, "The first 3D-printed and wet-metallized three-axis accelerometer with differential capacitive sensing," *IEEE Sensors J.*, vol. 19, no. 20, pp. 9131–9138, Oct. 2019.
[21] M. Arh, J. Slavič, and M. Boltežar, "Design principles for a single-process 3D-printed accelerometer—Theory and experiment," *Mech. Syst. Signal Process.*, vol. 152, May 2021, Art. no. 107475.
[22] M. Arh and J. Slavič, "Single-process 3D-printed triaxial accelerometer," *Adv. Mater. Technol.*, vol. 7, no. 7, Jul. 2022, Art. no. 2101321.
[23] A. Leoni, G. Barile, G. Ferri, and V. Stornelli, "Analysis and development technique of a fully 3-D-Printed differential capacitive anemometric sensor," *IEEE Sensors J.*, vol. 22, no. 20, pp. 19439–19454, Oct. 2022.
[24] G. Barile, L. Iacoboni, V. Stornelli, and G. Ferri, "Accelerometric system based on a fully FDM 3D printed sensor," in *Proc. SIE*, in Lecture Notes in Electrical Engineering. Cham, Switzerland: Springer, 2023, pp. 91–97, doi: 10.1007/978-3-031-26066-7_14.
[25] A. Depari, E. Sisinni, A. Flammini, G. Ferri, V. Stornelli, G. Barile, and F. R. Parente, "Autobalancing analog front end for full-range differential capacitive sensing," *IEEE Trans. Instrum. Meas.*, vol. 67, no. 4, pp. 885–893, Apr. 2018.
[26] A. De Marcellis, G. Ferri, and P. Mantenuto, "Analog Wheatstone bridge-based automatic interface for grounded and floating wide-range resistive sensors," *Sens. Actuators B, Chem.*, vol. 187, pp. 371–378, Oct. 2013.
[27] G. Ferri, F. R. Parente, V. Stornelli, G. Barile, and L. Pantoli, "Automatic bridge-based interface for differential capacitive full sensing," *Proc. Eng.*, vol. 168, pp. 1585–1588, Jan. 2016.
[28] G. Barile, G. Ferri, F. R. Parente, V. Stornelli, A. Depari, A. Flammini, and E. Sisinni, "A standard CMOS bridge-based analog interface for differential capacitive sensors," in *Proc. 13th Conf. Ph.D. Res. Microelectron. Electron. (PRIME)*, Jun. 2017, pp. 281–284, doi: 10.1109/PRIME.2017.7974162.
[29] G.-Q. Zhong, R. Bargar, and K. S. Halle, "Circuits for voltage tuning the parameters of Chua's circuit: Experimental application for musical signal generation," *J. Franklin Inst.*, vol. 331, no. 6, pp. 743–784, Nov. 1994.

GIANLUCA BARILE was born in Avezzano, Italy. He received the master's degree (cum laude) in electronics engineering and the Ph.D. degree from the University of L'Aquila, Italy, in 2016 and 2020, respectively. His research interests include sensors interfaces and integrated circuits, and system for industrial electronics.

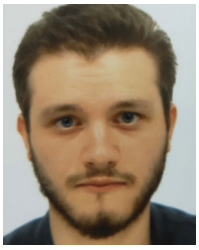

PAOLO ESPOSITO was born in Chieti, Italy. He received the master's degree in electronics engineering from the University of L'Aquila, Italy, in 2022, where he is currently pursuing the Ph.D. degree. His research interest includes the development of electronic interfaces for sensors.

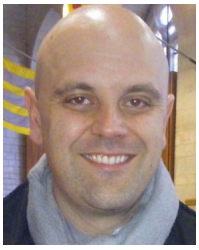

VINCENZO STORNELLI (Senior Member, IEEE) was born in Avezzano, Italy. He received the "Laurea" degree (cum laude) in electronic engineering, in 2004. In October 2004, he joined the Department of Electronic Engineering, University of L'Aquila, L'Aquila, Italy, where he is involved as an Associate Professor. His research interests include several topics in computational electromagnetics, including microwave antenna analysis for outdoor ultrawideband applications. He serves as a reviewer for several international journals and an Editor for the *Journal of Circuits, Systems, and Computers*.

GIUSEPPE FERRI (Senior Member, IEEE) was born in L'Aquila, Italy. He received the "Laurea" degree (cum laude) in electronic engineering, in 1988. In 1991, he joined the Department of Electronic Engineering, University of L'Aquila, L'Aquila, where he is currently a Full Professor in electronics and microelectronics. His research interests include the design of analog electronic circuits for integrated sensor applications both in voltage and in current-mode. In this field of research, he is the author or coauthor of seven patents, four international books, one book chapter, and more than 400 publications in international journals and conference proceedings. He is an Editor of *Sensors* and *Journal of Circuits, Systems, Computers*.

Open Access funding provided by 'Università degli Studi dell'Aquila' within the CRUI CARE Agreement